New insights on the protein-ligand interaction differences between the two primary cellular retinol carriers[S]

Lorella Franzoni,* Davide Cavazzini,[†] Gian Luigi Rossi,[1,†] and Christian Lücke[1,§]

Department of Experimental Medicine, Section of Chemistry and Structural Biochemistry,* and Department of Biochemistry and Molecular Biology,[†] University of Parma, Italy; and Max Planck Research Unit for Enzymology of Protein Folding,[§] Halle (Saale), Germany

Abstract **The main retinol carriers in the cytosol are the cellular retinol-binding proteins types I and II (CRBP-I and CRBP-II), which exhibit distinct tissue distributions. They play different roles in the maintenance of vitamin A homeostasis and feature a 100-fold difference in retinol affinity whose origin has not been described in detail. NMR-based hydrogen/deuterium exchange measurements show that, while retinol binding endows both proteins with a more rigid structure, many amide protons exchange much faster in CRBP-II than in CRBP-I in both apo and holo form, despite the conserved three-dimensional fold. The remarkable difference in intrinsic stability between the two homologs appears to modulate their binding properties: the stronger retinol binder CRBP-I displays a reduced flexibility of the backbone structure with respect to CRBP-II. This difference must derive from specific evolution-based amino acid substitutions, resulting in additional stabilization of the CRBP-I scaffold: in fact, we identified a number of potential salt bridges on the protein surface as well as several key interactions inside the binding cavity. Furthermore, our NMR data demonstrate that helix αII of the characteristic helix-turn-helix motif in the ligand portal region exists in both apo and holo CRBP-II. Hence, the previously proposed model of retinol binding needs to be revised.—** Franzoni, L., D. Cavazzini, G. L. Rossi, and C. Lücke. **New insights on the protein-ligand interaction differences between the two primary cellular retinol carriers. *J. Lipid Res.* 2010.** 51: **1332–1343.**

Supplementary key words β-barrel fold • cellular retinol-binding proteins • hydrogen/deuterium exchange • intracellular lipid-binding proteins • ligand affinity • nuclear magnetic resonance spectroscopy • structural stability

Retinoids are required for many essential physiological functions, such as cell growth and differentiation, morphogenesis, immunocompetence, and vision (1, 2). Because of their low solubility in aqueous media, these lipids are transported through blood and within cells by proteins that belong to the calycin superfamily (3–5). In the cytosol, specific members of the intracellular lipid-binding protein (i-LBP) family, the so-called cellular retinol-binding proteins (CRBPs) are involved in the uptake, storage, and metabolism of retinol. The most abundant carriers are the CRBP types I and II; they display a strikingly different tissue distribution and appear to play distinct roles in the maintenance of vitamin A homeostasis. CRBP-I, the most tightly retinol-binding carrier with an estimated K_d in the order of 0.1 nM (6), is widely expressed in various tissues (4, 7, 8), where it is involved in the membrane-mediated retinol uptake from plasma (9) and facilitates the synthesis and hydrolysis of retinyl esters (10–12). Moreover, CRBP-I is implicated in the intracellular trafficking of retinol and its delivery to the enzymes that catalyze its conversion to retinaldehyde (13, 14), which can be further oxidized to retinoic acid (15, 16). In contrast, CRBP-II, which binds retinol with ~100-fold lower affinity than CRBP-I (6), is expressed almost exclusively in the enterocytes, where it plays a pivotal role in the absorption and metabolism of vitamin A and β-carotene (4, 17, 18).

The members of the i-LBP family generally exhibit the same typical β-barrel fold, formed by two nearly orthogonal five-stranded β-sheets (A-E and F-J) and two short α-helices that are inserted between strands βA and βB. A possible "portal" for the ligand to enter the internal binding cavity has been identified in the region located between α-helix II and the turns βC-βD and βE-βF. Crystallographic studies have shown that the binding cavity is

Studies in Parma were supported by grants from the Ministero dell'Istruzione, dell'Università e della Ricerca to G.L.R. and from "Ricerca Scientifica di Ateneo FIL 2007" to L.F.

Manuscript received 7 September 2009 and in revised form 25 November 2009.

Published, JLR Papers in Press, November 25, 2009
DOI 10.1194/jlr.M002006

Abbreviations: CRBP, cellular retinol-binding protein; FABP, fatty acid binding protein; H/D, hydrogen/deuterium; HSQC, heteronuclear single-quantum coherence; i-LBP, intracellular lipid-binding protein; NOE, nuclear Overhauser effect; NOESY, nuclear Overhauser enhancement and exchange spectroscopy; TOCSY, total correlation spectroscopy.

[1] To whom correspondence should be addressed.
e-mail: gianluigi.rossi@unipr.it (G.L.R.);
luecke@enzyme-halle.mpg.de (C.L.)

[S] The online version of this article (available at http://www.jlr.org) contains supplementary data in the form of two figures and one table.

always filled with water molecules both in the absence and in the presence of the amphiphilic ligand. Despite the fact that the structural properties of the i-LBPs have been studied extensively (19), the detailed mechanisms of ligand uptake and targeted release, i.e., the fundamental functions of these carriers, remain obscure.

NMR investigations of various i-LBPs have revealed that their backbone dynamics are correlated with the respective binding properties (20, 21). It appears that the i-LBP family evolved from a multifaceted ancestral precursor into highly specialized lipid carriers that transport either retinoids or fatty acids through the cytosol of various tissues (22, 23).

The overall structure of CRBP-I complexed with all-*trans*-retinol is essentially identical in the crystal (24) and in solution (25). In particular, the binding cavity is fully shielded from the outside medium, as is the case also for the ligand-free form in solution, the only state in which the apo structure has been determined (25). Studies of the protein dynamics indicated that merely a few residues exhibit increased mobility on the picosecond-to-nanosecond timescale in apo with respect to holo CRBP-I (25), while a high degree of conformational exchange on the microsecond-to-millisecond timescale has been revealed (26), which is markedly reduced upon retinol binding. Using line shape analysis of NMR signals, we derived a mechanism of ligand binding that suggests that retinol, after an initial nonspecific encounter with the surface of apo CRBP-I, modulates site-specific mobility of the protein by inducing the formation of long-lived (millisecond to second) transiently open conformers in the portal region (27).

NMR studies of the apo CRBP-II solution structure (28) previously suggested a remarkable difference with respect to the crystal structure (29). Residues 27-34,[2] which in the crystal structure form the second α-helix of the i-LBP typical helix-turn-helix motif, did not appear to exhibit a helical conformation in solution (**Fig. 1**). This feature, in combination with an alternative orientation of the F57 side chain, seemed to render the binding cavity more accessible to the ligand. Upon retinol binding, changes both in the protein structure, including formation of helix αII, and in the backbone dynamics were reported (30). Here, we suggest that the NMR-based detection of helix αII may be affected by the experimental conditions; our data indicate that also in the absence of retinol, the segment F27-V34 adopts in solution predominantly a helical structure. As a consequence, the previously proposed model of ligand binding needs to be revised.

By performing hydrogen/deuterium (H/D) exchange experiments with both CRBP types, we compared the backbone stabilities of these two highly homologous proteins both in the apo and holo forms. The results indicate that the 100-fold stronger retinol binding of CRBP-I compared with CRBP-II is a consequence of rather specific evolution-based sequence differences, which affect the internal protein dynamics to optimize each carrier for its particular physiological function.

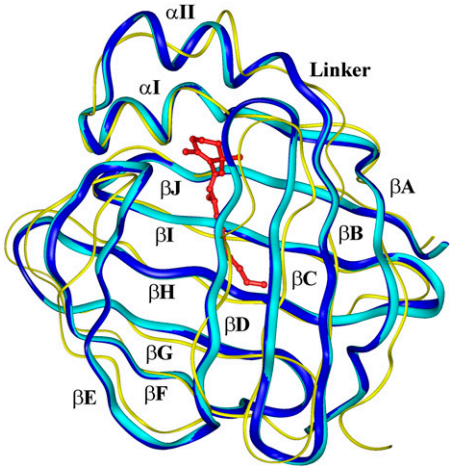

Fig. 1. Backbone ribbon superposition of the rat CRBP-II crystal structures in the apo (cyan; PDB ID code 1OPA) and holo form (blue; PDB ID code 1OPB). The overall protein fold consists of 10 antiparallel β-strands (A through J) and two short α-helices (I and II); bound retinol is shown in red. The two forms exhibit a nearly identical conformation. In addition, the solution structure of rat apo CRBP-II (yellow; PDB ID code 1B4M, conformer 1) is superposed with the crystal structures for comparison. This figure has been prepared with the program Insight II (Accelrys, San Diego, CA).

EXPERIMENTAL PROCEDURES

Protein expression and purification

The cDNA of rat CRBP-I was cloned into a pET-11b vector and expressed in the *Escherichia coli* BL21(DE3) strain. The bacteria were grown at 37°C in LB medium (M9 minimal medium with 5 mg/ml thiamine for ^{15}N-labeled samples) containing ampicillin (0.1 mg/ml) until the optical density reached ~0.6 at 600 nm. Overexpression of CRBP-I was induced by adding 1 mM isopropyl-1-thio-β-D-galactopyranoside. After an additional 5 h of growth (15 h for the labeled protein), the bacterial cells were harvested by centrifugation at 9,000 *g* for 10 min. The recombinant protein was purified to homogeneity as described elsewhere (31, 32). Briefly, the supernatant obtained from the bacterial lysate, after an ammonium sulfate fractionation step (50% saturation), was loaded on an Ultrogel AcA54 gel filtration column (Biosepra, Lockedrive, MA). Next, the protein was purified to homogeneity by elution with a linear NaCl gradient (0–400 mM) in 25 mM Tris-HCl buffer (pH 7.3), using a QMA anion-exchange FPLC column (Waters, Milford, MA). The purity of the protein was monitored by SDS-PAGE with 15% polyacrylamide gels. The protein concentration was determined using an extinction coefficient of 28,800 M^{-1} cm^{-1} at 280 nm (31).

The cDNA of rat CRBP-II was cloned into a pMON vector and expressed in the *E. coli* JM101 strain (33). The bacteria were grown at 30°C in LB medium (M9 minimal medium with 5 mg/ml thiamine for ^{15}N-labeled samples) containing ampicillin (0.1 mg/ml). When the optical density of the cell suspension reached ~0.2 at 600 nm, 0.05 mg/ml nalidixic acid was added to induce

[2]The numbering of the rat CRBP-I and CRBP-II sequences has been kept as reported in the crystal structure entries of the RCSB database, despite the fact that the N terminus of the recombinant proteins starts with an additional Met residue, which has been named Met-0.

protein expression. After an additional 4 h of growth (15 h for the labeled protein), the cells were harvested by centrifugation at 9,000 *g* for 10 min. CRBP-II was purified similarly to CRBP-I, except for an additional fractionation step at 70% ammonium sulfate saturation that causes precipitation of CRBP-II prior to gel filtration. The purity of the protein was monitored by SDS-PAGE with 15% polyacrylamide gels. The protein concentration was determined using an extinction coefficient of 25,500 M^{-1} cm^{-1} at 280 nm (31).

As previously reported, contamination by fatty acids is nearly negligible (<2%) in recombinant CRBP-I and CRBP-II (34). To prepare the holo proteins, all-*trans*-retinol solubilized in dimethylsulfoxide was added in 1.5 molar excess. Unbound retinol was removed by a Micro Bio-Spin 6 chromatography column (Bio-Rad, Hercules, CA). The reconstituted holo CRBP complexes exhibited A_{350}/A_{280} ratios close to the optimal values (i.e., equal to or higher than 1.6) that were reported for the natural proteins isolated directly from rat liver (8).

NMR data collection and processing

For NMR measurements, 1.3–1.4 mM protein samples were prepared in potassium phosphate buffer (20 mM, pH 6.0 or 7.4, 10% D_2O) containing 0.05% NaN_3. All NMR experiments were carried out at 25°C on Bruker DMX spectrometers operating at ^1H resonance frequencies of 499.87, 600.13, or 600.40 MHz, equipped with triple resonance ($^1H/^{13}C/^{15}N$) XYZ-gradient probes. For resonance assignments, homonuclear two-dimensional spectra [total correlation spectroscopy (TOCSY) and nuclear Overhauser enhancement and exchange spectroscopy (NOESY)] as well as ^{15}N-edited multidimensional spectra were acquired; the latter included 2D heteronuclear single-quantum coherence (HSQC) and 3D NOESY-HSQC. The TOCSY experiments were performed with spin lock times of either 80 or 6.6 ms. In the NOESY experiments, a mixing time (τ_m) of 150 ms was generally employed. All multidimensional spectra were recorded in a phase-sensitive mode with time-proportional phase incrementation of the initial pulse. Quadrature detection was applied, with the carrier placed in the center of the ^1H spectrum on the water resonance. All chemical shifts were referenced to external sodium 2,2-dimethyl-2-silapentane-5-sulfonate (Cambridge Isotope Laboratories, Andover, MA) in order to ensure consistency among the spectra (35).

The spectral data were processed on a Silicon Graphics O2 workstation using the Bruker XWIN-NMR 1.3 software package. A 90° phase-shifted squared sine-bell function was used for apodization in all dimensions. Polynomial baseline correction was applied to the processed spectra wherever necessary. Peak picking and data analysis of the transformed spectra were performed using the AURELIA 2.5.9 (Bruker) and FELIX 2000 (Accelrys, San Diego, CA) software packages.

For the identification of slow exchanging amide protons, the protein sample buffer was replaced with a perdeuterated solution consisting of 20 mM KD_2PO_4 and 0.05% NaN_3 in D_2O, as previously described (36). This perdeuterated solution was prepared from the protonated buffer (90% H_2O/10% D_2O) at pH 6.0 by lyophilizing and redissolving in D_2O twice. The buffer exchange was performed at 4°C with Vivaspin centrifugal concentrators (molecular weight cutoff of 10 kDa) in several rounds of filtration over 6–10 h. Following equilibration to 25°C inside the NMR magnet, a series of homonuclear TOCSY (alternating between 30 and 80 ms spin lock time) and NOESY (alternating between 80 and 150 ms mixing time) experiments were collected over a period of more than 9 days (the first 3.5 days at 600.13 MHz and the remaining time at 499.87 MHz) in order to monitor the amide proton exchange.

RESULTS

Structural comparison between apo and holo CRBP-II

The structural features of the ligand entry portal represent a key aspect of retinol uptake and release by CRBPs. In the case of CRBP-I in solution, the topology of the entry portal is essentially identical in the presence and absence of retinol (25). Similarly, apo and holo CRBP-II in the crystal exhibit only small differences in the backbone fold (29), with a very low total Cα trace root mean square deviation (0.23 Å), while in solution the helix αII segment of the typical helix-turn-helix motif has been described as unwound in the apo form (28). The reported discrepancy between the solution and crystal structures of apo CRBP-II (see Fig. 1) is remarkable because a mostly unwound helix αII would be unique in the entire i-LBP family. Moreover, the unfolded helix αII would likely facilitate retinol access to its binding site. Therefore, we aimed at investigating the conformational characteristics of the CRBP-II ligand entry portal under a variety of solution conditions.

Initially, we collected ^{15}N-edited multidimensional NMR experiments of apo and holo CRBP-II at 25°C and pH 6.0 (**Fig. 2A**) in order to avoid excessive line broadening as a result of amide proton exchange with water (37), since helix αII is highly solvent exposed in the i-LBP fold. In addition, homonuclear two-dimensional spectra were also analyzed to compensate for decreased spectral resolution in the indirectly detected ^1H dimensions of the 3D NOESY. Nearly all nuclear Overhauser effect (NOE) connectivities that are typical for an α-helix structure have been identified in the segment Phe27-Val34, both in the apo and holo form of the protein (Fig. 2B), albeit several NOE connectivities are ambiguous in the apo form due to a higher degree of chemical shift degeneracy of the Hα resonances. Nevertheless, the backbone NOE patterns observed at this pH support the presence of helix αII in both forms of CRBP-II.

Moreover, according to the chemical shift index approach (38), comparison of the Hα resonances with residue-specific values (**Table 1**) clearly indicates helix structure for all amino acids in this segment of apo CRBP-II, except Val-34. In the holo form, the Hα chemical shift values show a similar trend, except for the two C-terminal residues Ala-33 and Val-34, where the difference with respect to the random coil values is again small. Finally, comparison of the HN resonances in helix αII (Table 1) also reveals nearly identical chemical shift values between the apo and holo protein except for residues Ile-32, Ala-33, and Val-34, whose intrahelical hydrogen bonds might be affected by differences in conformational dynamics of the adjacent αII-βB linker upon retinol binding.

In order to examine whether these findings are valid also at a higher, more physiological pH, the above-described experiments were repeated at pH 7.4 like in the previous NMR study (28). As expected, the NOE pattern defining helix αII was less complete due to stronger line-broadening effects that affected mainly the weak long-distance NOE signals (Fig. 2C). However, the chemical shift values of the backbone HN and Hα resonances remained

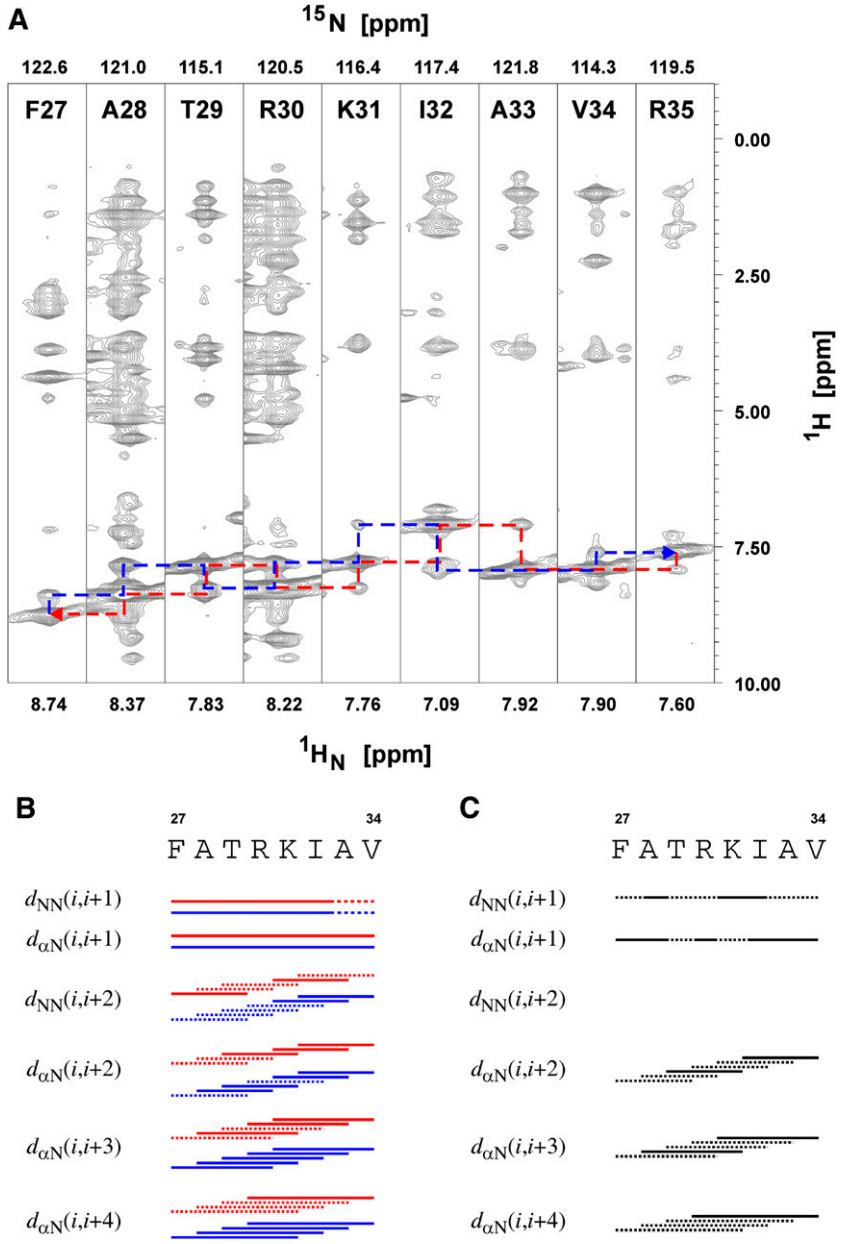

Fig. 2. A: Strip plot from a ^{15}N-edited 3D NOESY-HSQC spectrum of rat apo CRBP-II collected at pH 6.0 and 25°C. The dashed lines in red and blue connect the sequential HN-HN connectivities that are typical for helical conformation. B: The backbone NOE connectivity patterns of rat apo (red lines) and holo (blue lines) CRBP-II at pH 6.0 are shown in parallel for the segment Phe27-Val34. Dashed lines indicate ambiguous connectivities due to either spectral overlap, chemical shift degeneracy, or extremely weak signal intensity. Nearly all NOE signals that occur in the holo form are in principle also present in the apo protein. C: NOE pattern of rat apo CRBP-II at pH 7.4. Although the amide proton signal intensities are considerably weaker at this pH due to exchange broadening, NOE connectivities typical for helical structure are still observed.

nearly identical to those at pH 6.0 (differences ≤0.02 ppm), as shown in **Table 2**. Assuming that different conformational states may be populated in solution, the present NOE and chemical shift data imply that the segment F27-V34 adopts basically the same predominantly helical conformation at both pH 6.0 and 7.4. The global fold of the portal region in apo CRBP-II is therefore essentially identical to that of the holo form, as in the case of CRBP-I (25). Hence, rather than fundamental structural differences between the two homologous proteins, variations in their dynamics may be responsible for determining the ligand affinity.

Structural stability mapping of CRBP-I and CRBP-II based on H/D exchange

Previous studies with various i-LBPs have revealed a correlation between ligand-binding affinity and overall structural stability for several members of this protein family (21, 36). In order to determine whether such a correlation also applies to the cellular retinol carriers, we have now

TABLE 1. Comparison of backbone proton resonances (HN and Hα) in the αII-helix region between rat apo and holo CRBP-II at pH 6.0

Residue	HN_{apo}	$H\alpha_{apo}$	HN_{holo}	$H\alpha_{holo}$	$H\alpha_{coil}$[a]	$H\alpha_{apo}$-$H\alpha_{coil}$	$H\alpha_{holo}$-$H\alpha_{coil}$	HN_{apo}-HN_{holo}
Phe-27	8.76	3.93	8.86	3.89	4.42	−0.49	−0.53	−0.10
Ala-28	8.40	3.88	8.41	3.82	4.19	−0.31	−0.37	−0.01
Thr-29	7.86	3.89	7.93	3.69	4.37	−0.48	−0.68	−0.07
Arg-30	8.27	3.72	8.38	3.65	4.32	−0.60	−0.67	−0.11
Lys-31	7.80	3.83	7.84	3.73	4.23	−0.40	−0.50	−0.04
Ile-32	7.14	3.88	6.87	3.62	4.09	−0.21	−0.47	+0.27
Ala-33	7.95	3.95	8.29	4.12	4.19	−0.24	−0.07	−0.34
Val-34	7.92	4.05	8.22	4.12	4.11	−0.06	+0.01	−0.30

The Hα chemical shift values (in ppm) are compared with standard random coil values for each residue type; according to the chemical shift index approach (38), shift differences below −0.10 ppm indicate a helical conformation. The last column shows the differences in the HN resonances between the apo and holo forms
[a]Values taken from Ref. 54.

performed in an analogous manner NMR-based H/D exchange experiments on CRBP-I and CRBP-II in the ligand-free and retinol-bound forms.

In both proteins, the number of amide protons displaying slowed H/D exchange was larger in the holo than in the apo form (**Fig. 3A**; supplementary Table I), suggesting a more rigid overall protein structure in the presence of ligand, as previously observed also for other members of the i-LBP family (19). By comparing apo and holo CRBP-I, the most pronounced differences appear in strands βD, βE, at the start of βF, at the ends of βC and βG, and in the turn between helices αI and αII. All these segments are located around the portal (Fig. 3B), thus confirming that the bound retinol stabilizes this region. This increase of backbone stability upon ligand binding occurs also at the residues belonging to the turn βE-βF, whose amide proton resonances could not be assigned in the apo form because of a high degree of conformational mobility (25), whereas the two other structural elements that define the portal (i.e., helix αII and turn βC-βD) both exhibit very fast H/D exchange with hardly any differences between the apo and holo forms.

The local flexibility of apo and holo CRBP-I had been probed and mapped previously by mass spectrometry employing limited proteolysis; the reduction of deuterium labeling upon formation of the complex was attributed to a retinol-dependent increase of conformational stability in specific regions rather than to a direct shielding of amide hydrogens by the ligand (39). Based on the NMR-derived data, we can now specify that the higher deuteration observed with mass spectrometry in segments 28-49 and 70-84 of the apo form with respect to the holo form (39) is restricted *i*) to helix αII (residues 28–34), which features high flexibility and solvent exposure throughout the i-LBP family, *ii*) to the linker αII-βB (residues 35–37), *iii*) to the turn βB-βC (residues 45–48), and *iv*) to the turn βE-βF (residues 75–79), while it does not occur in the β-strand sections (i.e., residues 38–44, 49, 70–74, and 80–84). The more limited regions identified in the present work are all part of the portal, except for the turn βB-βC.

TABLE 2. Comparison of the backbone proton resonances (HN and Hα) in the αII-helix region of rat apo CRBP-II at pH 6.0 and 7.4

	pH 6.0		pH 7.4		pH 6.0–7.4	
Residue	HN	Hα	HN	Hα	HN	Hα
Phe-27	8.76	3.86	8.76	3.86	±0.00	±0.00
Ala-28	8.40	3.88	8.40	3.86	±0.00	+0.02
Thr-29	7.86	3.89	7.85	3.88	+0.01	+0.01
Arg-30	8.27	3.72	8.27	3.71	±0.00	+0.01
Lys-31	7.80	3.83	7.79	3.81	+0.01	+0.02
Ile-32	7.14	3.88	7.12	3.86	+0.02	+0.02
Ala-33	7.95	3.95	7.97	3.93	−0.02	+0.02
Val-34	7.92	4.05	7.93	4.03	−0.01	+0.02

Apo and holo CRBP-II exhibited a behavior similar to that described for CRBP-I. However, many backbone amide protons that are involved in the hydrogen bond interactions of the secondary structure elements show a considerably faster exchange in CRBP-II, especially in the ligand-free form (Fig. 3).

Comparing the apo forms of CRBP-I and CRBP-II, clear differences in the H/D exchange times are observed at the end of strand βA, at the start of βB, in the entire strand βC (all belonging to the first β-sheet), in the middle of strand βF, in helix αI, and at residues 92 and 124. Helix αI is linked directly to helix αII, which is part of the ligand entry portal. Strand βC, which leads to the turn βC-βD within the portal, exhibits the highest difference in sequence between the two CRBP types (supplementary Fig. I), resulting in altered electrostatic surface potentials that affect salt bridge formations as discussed in the next section. Residues 92 and 124 reside in the turns βF-βG and βI-βJ, respectively, which are both stabilized by salt bridges that occur only in CRBP-I (see below).

The difference in the amide exchange times of helix αI between the two CRBP types becomes less pronounced upon retinol binding, presumably due to the stabilizing effect of the ligand. It must be noted that the turn βE-βF, which is also part of the portal, appears to be more stabilized in holo CRBP-I than in holo CRBP-II. A possible reason for this effect could be the D79G substitution, assuming that the Gly residue favors a higher structural flexibility of the turn βE-βF in CRBP-II. Moreover, the substitutions L29T (helix αII) and P38Q (linker αII-βB) in CRBP-II both cause a loss of hydrophobic contacts between the protein and the β-ionone ring of the bound retinol: the nonpolar van der Waals contacts of the Leu-29 side chain are lost because the methyl group of Thr is not as far-reaching (i.e., the interatom distances between retinol and Thr-29 exceed 3.5 Å), and Pro-38 is replaced by a polar moiety.

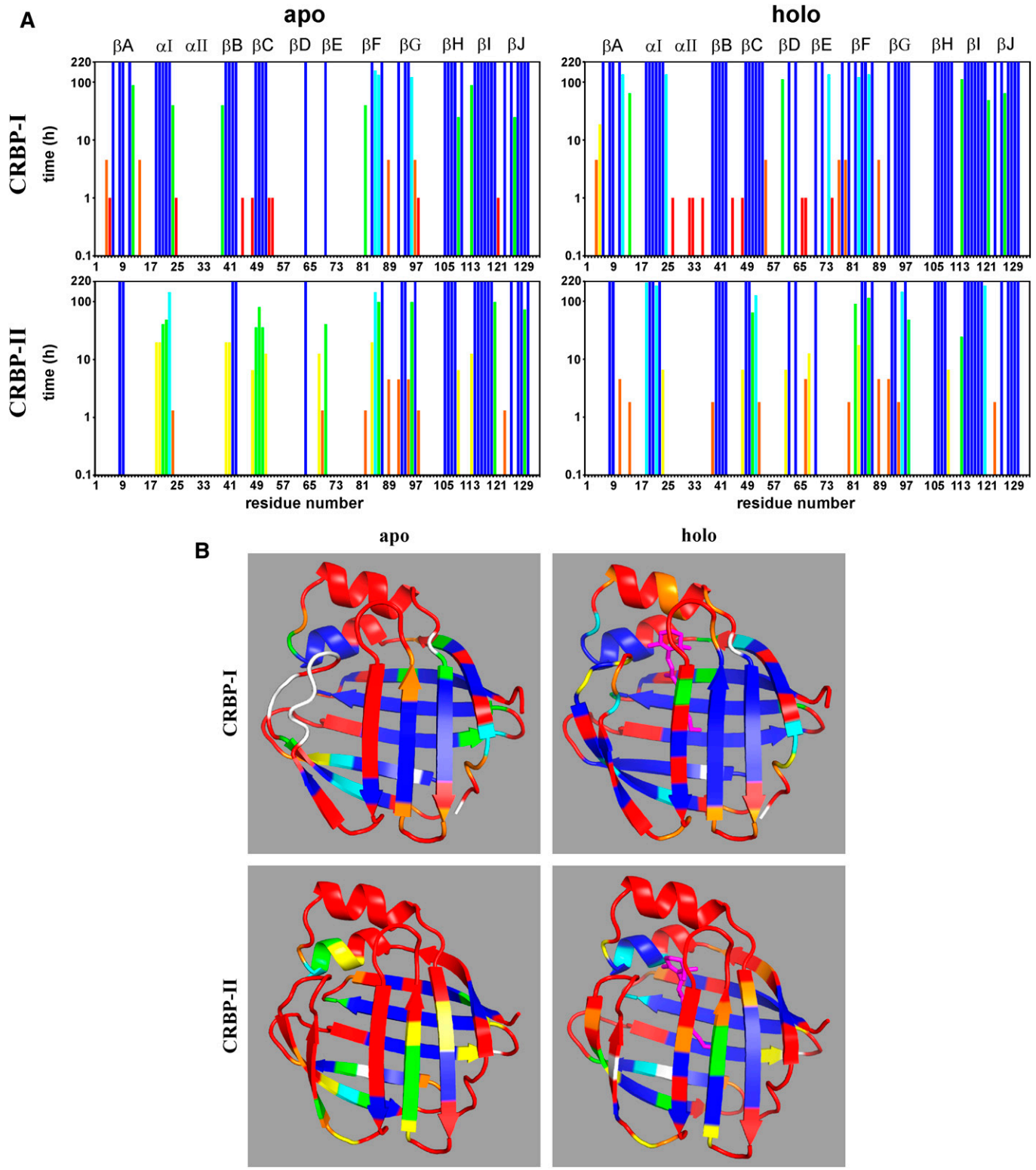

Fig. 3. A: The logarithmic bar graphs show the maximal observation times (in hours) of the CRBP-I and CRBP-II backbone amide proton resonances after transfer to perdeuterated buffer (color coding: red ⩽1 h; orange = 1–5 h; yellow = 5–24 h; green = 1–5 days; cyan = 5–9 days; blue ⩾9 days). NMR spectra of both the apo and holo forms were collected at 25°C in regular intervals, following 6–10 h of buffer exchange at 4°C. One-hour TOCSY spectra were acquired every 9–15 h, with 1D spectra collection every 4 h in between, for a total period of 220 h. B: Intervals of backbone amide proton exchange mapped onto the protein backbone ribbon of CRBP-I and CRBP-II with the same color coding as in A. Residues colored white could not be analyzed due to either missing assignments (Glu-72, Asp-73, Leu-74, Thr-75, Gly-76, Asp-79, and Arg-80 in apo CRBP-I; Leu-93 in apo and holo CRBP-I; Glu-72 in holo CRBP-II), extreme line broadening (Cys-95 and Glu-111 in apo and holo CRBP-II), or lack of amide protons (Pro-1 and Pro-38 in CRBP-I). The retinol ligand is shown in magenta. This figure has been prepared with the program Pymol (DeLano Scientific, Palo Alto, CA) using the solution structures of rat CRBP-I (PDB 1JBH and 1KGL) and the crystal structures of rat CRBP-II (PDB 1OPA and 1OPB).

Sequence comparison between CRBP-I and CRBP-II: a key to understanding their differences in structural stability

The surface residues. Given the very similar three-dimensional fold and identical secondary structure elements of the two proteins (backbone root mean square deviation of 0.6 Å between rat holo CRBP-I and CRBP-II), the marked differences in structural stability must be related to variations in the primary structure. Despite a very close evolutionary relationship between the CRBP homologs (22), their amino acid sequences show only 56% identity and 70% homology (**Fig. 4**; supplementary Fig. I). Most sequence differences occur at residues whose side chains are located on the protein surface. More precisely, out of 86 surface-exposed residues (not counting residue His-134 in CRBP-I), 45 are altered. Considering all histidines as polar but noncharged, these 45 differences are subdivided as follows: 12 maintain the same polarity or charge, four correspond to a switch from polar to nonpolar, four to a switch from nonpolar to polar, and 25 are associated with a change in charge. In fact, two complete reversals of charge occur at residues 9 (positive to negative) and 114 (negative to positive). In total, all these side chain replacements entail that CRBP-I has three negatively charged residues in excess over CRBP-II and two positively charged residues less than CRBP-II, leading to a net charge difference of 5: CRBP-I has a total charge of −7 and CRBP-II of −2. Although this difference in total charge does not have significant consequences on the electrostatic surface potential maps of the two proteins (not shown), the extensive variations in the charge positions could be the reason for the differences observed in their acid denaturation behavior (40).

CRBP-I contains a salt bridge between Asp-89 and Lys-92 (Fig. 4), which is common within the i-LBP family and apparently stabilizes the β-turn FG. CRBP-II lacks this salt bridge because of the substitution K92T. Moreover, based on ion pair distances obtained from X-ray coordinates, the charge differences between rat CRBP-I and CRBP-II can result in additional salt bridges that occur in either one of

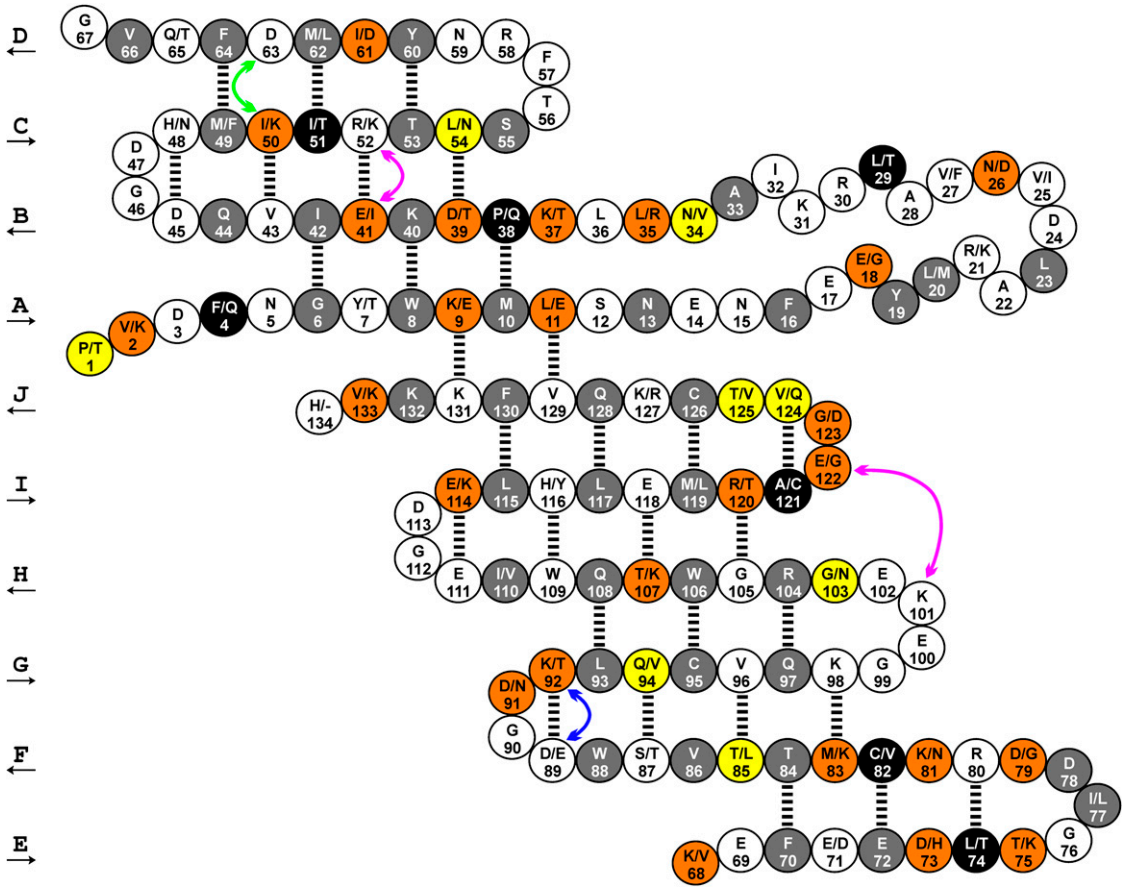

Fig. 4. Schematic representation of the secondary structure alignment between CRBP-I and CRBP-II from rat. Each circle represents a residue; in the case of an amino acid substitution, the first letter denotes the residue in CRBP-I and the second letter the corresponding residue in CRBP-II. The antiparallel β-strands A through J (labeled in the left margin) are arranged in straight rows with hashed lines indicating hydrogen bonds. The α-helices I and II (residues 16–23 and 27–34, respectively) are sketched in a skew array. Gray and black circles represent residues whose side chains are buried in the protein interior; black points out a nonconservative substitution between the two proteins. White, yellow, and orange circles represent residues with side chains at the protein surface; yellow marks substitutions from nonpolar to polar or vice versa, whereas orange denotes substitutions that involve changes in charge. (All His residues were considered as noncharged.) The additional salt bridge between Asp-89 and Lys-92 in CRBP-I is represented by a double arrow in blue. Other potential salt bridges are indicated by double arrows in magenta (for CRBP-I) and green (for CRBP-II).

the homologs: two in CRBP-I between Glu-41 and Arg-52 as well as between Lys-101 and Glu-122, and one in CRBP-II between Lys-50 and Asp-63 (Fig. 4). However, the latter is likely to stabilize the portal less efficiently than the one between Glu-41 and Arg-52 because it is located farther away from the turn βC-βD. This different salt bridge pattern on the surface is likely one of the reasons accounting for the higher stability of CRBP-I with respect to CRBP-II.

The buried residues. A critical factor for the structural stability of i-LBPs is a cluster of structural water molecules inside the binding cavity, which developed during the course of an evolutionary specialization of this protein family (23). These water molecules form an intricate network of hydrogen bonds among each other and with several side chains in the protein interior, thereby strengthening the overall protein structure as previously demonstrated by H/D exchange experiments performed with other i-LBPs (21).

Both CRBP types contain a comparable number of internal water molecules (seven in holo CRBP-I versus six in holo CRBP-II), located in similar positions (**Fig. 5A**). As reported earlier, an NMR signal belonging to the Lys-40 NζH side chain amide group (which is usually not observed due to solvent exchange) had been detected in the $^{1}H/^{15}N$-HSQC spectra of both apo and holo CRBP-I, indicating a slowed exchange of these amino protons both in the presence and in the absence of the ligand (25). Similarly, we detected the Lys-40 NζH signal both in apo and holo CRBP-II (supplementary Fig. II), in agreement with the hypothesis that the microenvironment of ordered water molecules inside the cavity is quite similar in both proteins. According to X-ray structure analysis, the Lys-40 NζH amino group has hydrogen bond contacts to a structural water molecule and to Thr-53 Oγ. In addition, the crystal structure of human holo CRBP-II indicates a possible second binding conformation where also the retinol hydroxyl group is hydrogen bonded to Lys-40 NζH (41). Upon addition of the ligand, the Lys-40 NζH amino group of CRBP-II displays an upfield shift from 7.33/30.7 ppm to 7.13/30.6 ppm in the $^{1}H/^{15}N$-HSQC spectra; this is presumably due to a shielding effect by the conjugated π-electron field of the retinol polyisoprene tail, as previously reported also in the case of CRBP-I (25).

Only 13 out of 47 residues whose side chains are located in the protein interior are altered between CRBP-I and II, but without any differences in charge (Fig. 4; supplementary Fig. I): six are nonpolar residues in both proteins, six are nonpolar in CRBP-I but polar in CRBP-II, and one is polar in CRBP-I but nonpolar in CRBP-II. Therefore, only seven substitutions are nonconservative. The substitutions L29T and P38Q, involving residues in contact with retinol, were discussed in the previous section; the substitution A121C is located in the β-turn IJ, where the neighboring residue 122 can form a salt bridge only in CRBP-I. The four remaining nonconservative substitutions F4Q, I51T, L74T, and C82V, all involving the internal network of structural water molecules described for heart fatty acid binding protein (FABP) (23), could be of particular relevance for protein stability, as they might affect this water cluster at the bottom of the binding cavity and, consequently, the entire protein scaffold.

The gap region. Another important structural feature of the i-LBPs is the so-called "gap", an interruption in the β-sheet where no direct backbone-to-backbone hydrogen bond contacts exist between β-strands D and E (Fig. 5B). This gap region is generally stabilized at the bottom by a structural water molecule (42) that forms hydrogen bonds to the backbone oxygens of residues 65 and 68 (both in the turn βD-βE) as well as to the backbone amide group of residue 86 (in β-strand F). Just above this water molecule, the highly conserved phenylalanines 64 and 70 show a skewed ring-stacking interaction (4 Å). Further stabilization may be provided by three structural water molecules that, in the case of rat holo CRBP-I and II, interconnect β-strands D and E in the upper part of the gap and, at the same time, are connected via Tyr-60 OηH and Glu-72 Oε2 to the above-mentioned internal water network.

Remarkably, the gap is considerably broader in all the available CRBP-II crystal structures in comparison to the only available CRBP-I crystal structure. The distance between the carbonyl oxygen atoms of residues 61 and 73 ranges between 6.3 and 8.1 Å in rat and human CRBP-II compared with 5.67 Å in holo CRBP-I. Moreover, the Tyr-60 hydroxyl group is shifted by about 1 Å only in CRBP-I, just like the Glu-72 Oε2 atom, which shows a concomitant tilt of its carboxylate group by ~40°. Hence, it appears that β-strands D and E are somehow pulled closer together in CRBP-I, thereby furnishing the protein with an increased structural stability.

An explanation for the above-described structural discrepancy in the gap region is found in the protein interior. In both CRBP types, Tyr-60 OηH is hydrogen bonded to Glu-72 Oε2, whose carboxylate group is part of a circular network of hydrogen bonds within the ligand-binding cavity that includes four internal water molecules as well as the side chains of residues Tyr-19 and Gln-97 (Fig. 5C). In addition, the side chains of Arg-104 and Trp-106 are also part of this internal hydrogen bond network, which is quite similar in the two CRBP types. However, this region of the protein interior also contains three residues (51, 62, and 74 in β-strands C, D, and E, respectively) that are different in CRBP-I and CRBP-II. These three residues endow CRBP-I with a more dense packing due to the longer hydrophobic side chains of Ile-51, Met-62, and Leu-74 compared to Thr, Leu, and Thr, respectively, in rat CRBP-II. Moreover, in human CRBP-II the water molecule between Glu-72 and Trp-106 is shifted significantly because of the additional space provided by the shorter Val-62 side chain, compared to Leu-62 in the protein from rat.

The nonconservative substitutions I51T and L74T were already mentioned with respect to the internal network of structural water molecules, which acts in several members of the i-LBP family as a kind of hydration shell for the hydrophobic residues inside the ligand-binding cavity (23). The presence of Met (in CRBP-I) instead of either Leu (in rat CRBP-II) or Val (in human CRBP-II) at position 62 is of

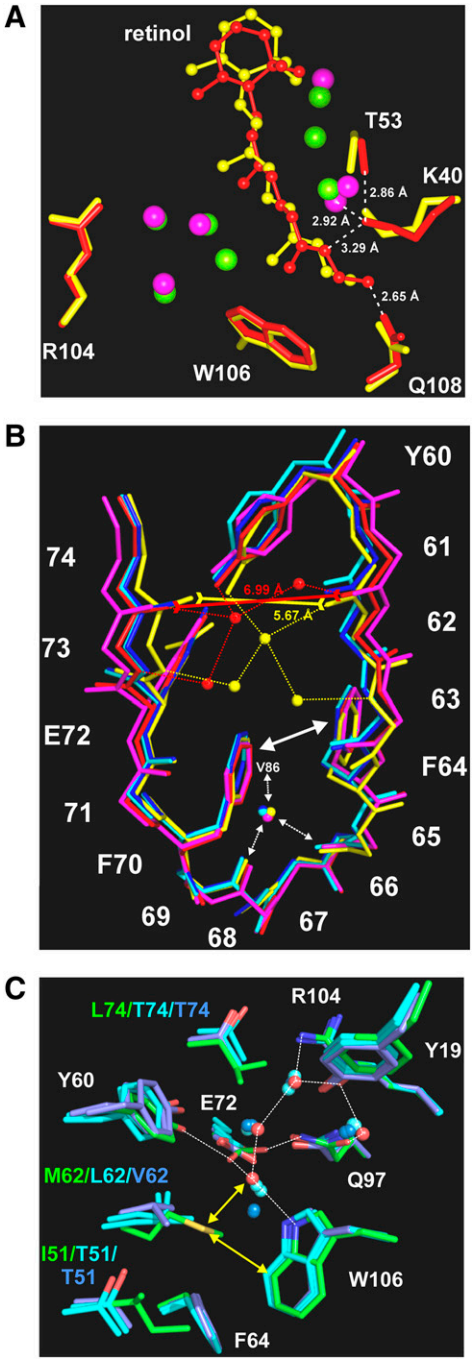

Fig. 5. A: Structural comparison of the water-filled binding cavities in rat holo CRBP-I (yellow with waters in green; PDB 1CRB) and rat holo CRBP-II (red with waters in magenta; PDB 1OPB). In both CRBP types, the internal residues and water molecules surrounding the bound ligand are located in similar positions. The distances relating to *i*) retinol binding to Gln-108 and *ii*) the Lys-40 NζH contacts are shown for CRBP-II. B: Structural comparison of the gap region between rat holo CRBP-I (yellow; PDB 1CRB), rat holo CRBP-II (red; PDB 1OPB), rat apo CRBP-II (magenta; PDB 1OPA), human holo CRBP-II (blue; 2RCT), and human apo CRBP-II (cyan; 2RCQ). The solid yellow and red lines indicate the distance between Ile-61 O and Asp-73 O in rat holo CRBP-I and CRBP-II. The dashed lines show hydrogen bond contacts within structural water networks that connect β-strands D and E in rat holo CRBP-I and CRBP-II. (The water molecules present in the other CRBP-II structures are not displayed here for easier viewing.) The solid double arrow indicates the ring-stacking interaction between Phe-64 and Phe-70. Dashed double arrows denote the hydrogen bond contacts of the structural water molecule at the bottom of the gap (Val-86 is not shown in this figure). C: Structural comparison of the region associated with the internal water network in rat holo CRBP-I (green; PDB 1CRB), rat apo and holo CRBP-II (cyan; PDB 1OPA and 1OPB), as well as human apo and holo CRBP-II (blue; 2RCQ and 2RCT). Dashed white lines denote the hydrogen bond network in CRBP-I. Yellow double arrows indicate nonbonded interactions of Met-62 Sδ. Conserved residues are labeled in white; substituted residues are marked in the colors of the respective structures. The more bulky side chains of residues Ile-51, Met-62, and Leu-74 furnish CRBP-I with a more dense packing in this part of the protein interior.

particular interest because of the divalent sulfur atom. Although the Met side chain is a poor hydrogen bond acceptor, as an electrophile it can form nonbonded interactions with electron-rich neighbors, such as oxygen atoms or aromatic rings (43). In the case of CRBP-I, the Met-62 side chain of β-strand D is located in a highly hydrophobic environment, sandwiched between the aromatic rings of Tyr-60 and Phe-64 and positioned just opposite to Ile-51 of β-strand C. Its Sδ atom is in close contact with the indole ring edge of Trp-106 (4.0 Å) and with the structural water molecule (3.3 Å) that is hydrogen bonded to Trp-106 Nε1. This arrangement presumably bestows further stability to this region via nonbonded S…Ar and S…O interactions, in addition to the above-described tighter packing in CRBP-I with respect to CRBP-II. Hence, it appears that the protein scaffold of CRBP-I is more compact, thus contributing to its increased structural stability compared with CRBP-II. A similar protein destabilization as a result of Met replacement has been reported for two Met-to-Leu mutants of T4 lysozyme, where each methionine residue is buried next to a Trp ring and at least one other aromatic moiety (44).

DISCUSSION

The retinol affinities of CRBP-I and CRBP-II differ considerably despite the fact that their overall three-dimensional fold as well as the ligand-binding motif (Lys-40, Trp-106, and Gln-108) are basically identical. The origin of this difference has not been described in detail to date, although previous studies have suggested that local conformational flexibility is likely to play a role (14, 45). In the case of CRBP-I, various residues in the region designated as the "helical cap" were investigated earlier by single site-directed mutagenesis (14), to determine their role in retinol affinity and in the efficiency of protein-bound retinol as substrate in retinal biosynthesis. The holo forms of all the respective CRBP-I variants displayed a more relaxed conformation at the helical cap, based on partial protease digestion; in terms of retinol affinity, the mutants showed K_d values either similar to the wild type or merely 2–5-fold higher (14). These results did not reveal any simple relationships among the measured factors, indicating that the examined surface residues contribute in varying degrees. A different study, applying ^{15}N relaxation measurements, suggested that conformational flexibility in the

putative portal region (helix αII and βC-βD turn) likely contributes to the interaction of CRBPs with ligands and retinoid metabolizing enzymes (45). However, the overall backbone structures of both the apo and holo forms were fairly rigid on the pico-to-nanosecond timescale (25, 28, 30, 45), while conformational exchange on the slower micro-to-millisecond timescale could be compared only for the ligand-free forms of the two proteins, due to its nearly complete suppression upon retinol binding (26, 45).

Our results provide new details, as the real-time NMR time frame covered by the H/D exchange measurements revealed significant differences between the two homologous proteins in the flexibility of certain secondary structure elements that were not previously addressed. The number of backbone amide protons that display slowed H/D exchange is considerably larger in CRBP-I than in CRBP-II, both in the absence and in the presence of the ligand, thus indicating a generally higher structural stability of CRBP-I relative to CRBP-II. CRBP stability and ligand affinity are thus correlated, as previously shown for other members of the i-LBP family (21, 36). This circumstance apparently results from a combination of stabilizing factors, which are the consequence of specific sequence differences that alter the pattern of potential salt bridges at the protein surface and affect key interactions inside the protein cavity involving the network of structural water molecules. These ordered waters are a crucial factor in the internal dynamics of all i-LBPs, as their interactions with the polypeptide chain represent an important aspect of structure, stability, and, as a consequence, ligand binding.

Does ligand affinity relate to the mechanisms of ligand uptake and targeted release? While the binding of retinol to apo CRBP-I is modulated by changes in the protein dynamics around the portal region that are induced by an initial nonspecific interaction of the ligand with the protein surface (27), experiments in progress indicate that retinol binding to CRBP-II does not require such an activation step. Distinct mechanisms of retinol delivery to model membranes have been reported for the holo forms of the two CRBP types (46). While CRBP-I as well as heart, brain, intestinal, and adipocyte FABP require a "transient collision-based mechanism," CRBP-II and liver FABP operate by an "aqueous diffusion-mediated mechanism" (47–49). In the case of intestinal and liver FABP, this difference pertains to ligand uptake from model membranes as well (50). These data correlate with the H/D exchange data, which have revealed that stronger ligand binding i-LBPs, such as heart, brain, and intestinal FABP as well as CRBP-I, exhibit a considerably higher structural stability than i-LBPs with lower ligand affinity, such as CRBP-II, epidermal and liver FABP, as well as the ileal lipid binding protein (21, 36, 51, 52). In the case of the CRBPs, whose K_d values differ by no more than two orders of magnitude in the nM range, the differences in H/D exchange behavior are not as dramatic as, for example, between heart FABP and the ileal lipid binding protein, whose K_d values are in the nM range (H/D exchange completed in several days) and in the μM range (H/D exchange completed within several hours), respectively. Taken together, these data thus suggest that i-LBPs featuring a more rigid structure and a higher ligand-binding affinity require for ligand uptake and release an activation step that causes a conformational rearrangement and/or a modulation of dynamics in the portal region. Other i-LBPs, which are endowed with higher conformational flexibility, allow for a "diffusion-mediated" ligand exchange between the binding cavity and the surrounding medium.

This study also suggests that the comparison of NMR data collected under a variety of solution conditions allows a better characterization of certain protein domains. Contrary to an earlier report on the solution structure of rat apo CRBP-II, suggesting an increased accessibility to the retinol binding cavity due, in part, to the unwinding of helix αII (28), our NMR results show that the segment F27-V34 does adopt a helical conformation, in agreement with the crystal structures of rat and human apo CRBP-II (29, 41). Apparently, the experimental conditions in the previous NMR study (28) did not allow the observation of several crucial NOE connectivities, thus pointing to a disordered conformation rather than to a helical fold. Other members of the i-LBP family also featured weak signal intensities of the backbone amides belonging to helix αII, as they frequently either exhibit strong line-broadening or exist as several distinct spin systems (21, 25, 51, 53). This may be the consequence of a high degree of conformational variability observed in this specific segment of the apo protein (26, 45) and/or a fast exchange of the amide protons with water, as helix αII exhibits a more pronounced solvent exposure than the other secondary structure elements of the typical i-LBP fold. We were able to identify the characteristic NOE connectivities that define helix αII by collecting NMR data at different pH values and taking advantage of the higher spectral resolution of homonuclear 2D-NOESY spectra, which were analyzed in combination with ^{15}N-edited 3D-NOESY data. Hence, the previously suggested structural implications for the mechanism of retinol binding to CRBP II (28), including a ligand-induced coil-to-helix transition (30), need to be reconsidered.

In conclusion, this study provides new evidence that in solution the global fold of the portal region in apo CRBP-II is very similar to that of CRBP-I. Furthermore, our results show that the distinctions in local flexibility between the two primary cellular retinol carriers are not restricted to helix αII and the turn βC-βD, but occur also in helix αI and in β-strands A through F. These differences in structural stability, which are a result of evolution-based sequence alterations, apparently modulate the overall binding properties of the two homologous CRBPs. Stiffening of the backbone upon ligand binding is presumably necessary to guarantee both protein complexes a certain stability during retinol transport. The fact that helix αII represents the secondary structure element with the highest flexibility in the holo form of both proteins could be an important feature to assist a transient conformational change that opens the portal during ligand release, a process that is likely promoted by external factors, such as specific protein-protein or protein-membrane interactions.

Prof. Jochen Balbach (University Halle-Wittenberg, Germany) and the European Large Scale Facility for Biomolecular NMR under the direction of Prof. Heinz Rüterjans (University of Frankfurt, Germany) are both gratefully acknowledged for the use of their NMR equipment.

REFERENCES

1. Gudas, L. J., M. B. Sporn, and A. B. Roberts. 1994. Cellular biology and biochemistry of the retinoids. *In* The Retinoids: Biology, Chemistry, and Medicine. 2nd edition. M. B. Sporn, A. B. Roberts, and D. S. Goodman, editors. Raven Press, New York. 443–520.
2. Blomhoff, R., and H. K. Blomhoff. 2006. Overview of retinoid metabolism and function. *J. Neurobiol.* **66:** 606–630.
3. Ong, D. E., M. E. Newcomer, and F. Chytil. 1994. Cellular retinoid-binding proteins. *In* The Retinoids: Biology, Chemistry, and Medicine. 2nd edition. M. B. Sporn, A. B. Robert, and D. S. Goodman, editors. Raven Press, New York. 283–317.
4. Li, E., and A. W. Norris. 1996. Structure/function of cytoplasmic vitamin A-binding proteins. *Annu. Rev. Nutr.* **16:** 205–234.
5. Noy, N. 2000. Retinoid-binding proteins: mediators of retinoid action. *Biochem. J.* **348:** 481–495.
6. Li, E., S. J. Qian, N. S. Winter, A. d'Avignon, M. S. Levin, and J. I. Gordon. 1991. Fluorine nuclear magnetic resonance analysis of the ligand binding properties of two homologous rat cellular retinol-binding proteins expressed in *Escherichia coli*. *J. Biol. Chem.* **266:** 3622–3629.
7. Bashor, M. M., D. O. Toft, and F. Chytil. 1973. *In vitro* binding of retinol to rat-tissue components. *Proc. Natl. Acad. Sci. USA.* **70:** 3483–3487.
8. Ong, D. E., and F. Chytil. 1978. Cellular retinol-binding protein from rat liver. Purification and characterization. *J. Biol. Chem.* **253:** 828–832.
9. Sundaram, M., A. Sivaprasadarao, M. M. DeSousa, and J. B. C. Findlay. 1998. The transfer of retinol from serum retinol-binding protein to cellular retinol-binding protein is mediated by a membrane receptor. *J. Biol. Chem.* **273:** 3336–3342.
10. Ottonello, S., S. Petrucco, and G. Maraini. 1987. Vitamin A uptake from retinol-binding protein in a cell-free system from pigment epithelial cells of bovine retina. Retinol transfer from plasma retinol-binding protein to cytoplasmic retinol-binding protein with retinyl-ester formation as the intermediate step. *J. Biol. Chem.* **262:** 3975–3981.
11. Herr, F. M., and D. E. Ong. 1992. Differential interaction of lecithin-retinol acyltransferase with cellular retinol binding proteins. *Biochemistry.* **31:** 6748–6755.
12. Ghyselinck, N. B., C. Bavik, V. Sapin, M. Mark, D. Bonnier, A. D. Hindelang, C. B. Nilsson, H. Hakansson, P. Sauvant, V. Azais-Braesco, et al. 1999. Cellular retinol-binding protein I is essential for vitamin A homeostasis. *EMBO J.* **18:** 4903–4914.
13. Posch, K. C., M. H. Boerman, R. D. Burns, and J. L. Napoli. 1991. Holocellular retinol binding protein as a substrate for microsomal retinal synthesis. *Biochemistry.* **30:** 6224–6230.
14. Penzes, P., and J. L. Napoli. 1999. Holo-cellular retinol-binding protein: distinction of ligand-binding affinity from efficiency as substrate in retinal biosynthesis. *Biochemistry.* **38:** 2088–2093.
15. Ross, A. C. 1993. Overview of retinoid metabolism. *J. Nutr.* **123** (Suppl. 2): 346–350.
16. Napoli, J. L. 1999. Retinoic acid: its biosynthesis and metabolism. *Prog. Nucleic Acid Res. Mol. Biol.* **63:** 139–188.
17. Ong, D. E. 1984. A novel retinol-binding protein from rat. Purification and partial characterization. *J. Biol. Chem.* **259:** 1476–1482.
18. Wongsiriroj, N., R. Piantedosi, K. Palczewski, I. J. Goldberg, T. P. Johnston, E. Li, and W. S. Blaner. 2008. The molecular basis of retinoid absorption: a genetic dissection. *J. Biol. Chem.* **283:** 13510–13519.
19. Lücke, C., L. H. Gutiérrez-González, and J. A. Hamilton. 2003. Intracellular lipid binding proteins: evolution, structure, and ligand binding. *In* Cellular Proteins and Their Fatty Acids in Health and Disease. A. K. Duttaroy and F. Spener, editors. Wiley-VCH, Weinheim, Germany. 95–118.
20. Lücke, C., D. Fushman, C. Ludwig, J. A. Hamilton, J. C. Sacchettini, and H. Rüterjans. 1999. A comparative study of the backbone dynamics of two closely related lipid binding proteins: bovine heart fatty acid binding protein and porcine ileal lipid binding protein. *Mol. Cell. Biochem.* **192:** 109–121.
21. Gutiérrez-González, L. H., C. Ludwig, C. Hohoff, M. Rademacher, T. Hanhoff, H. Rüterjans, F. Spener, and C. Lücke. 2002. Solution structure and backbone dynamics of human epidermal-type fatty acid-binding protein (E-FABP). *Biochem. J.* **364:** 725–737.
22. Schaap, F. G., G. J. van der Vusse, and J. F. Glatz. 2002. Evolution of the family of intracellular lipid binding proteins in vertebrates. *Mol. Cell. Biochem.* **239:** 69–77.
23. Lücke, C., S. Huang, M. Rademacher, and H. Rüterjans. 2002. New insights into intracellular lipid binding proteins: the role of buried water. *Protein Sci.* **11:** 2382–2392.
24. Cowan, S. W., M. E. Newcomer, and T. A. Jones. 1993. Crystallographic studies on a family of cellular lipophilic transport proteins. *J. Mol. Biol.* **230:** 1225–1246.
25. Franzoni, L., C. Lücke, C. Pérez, D. Cavazzini, M. Rademacher, C. Ludwig, A. Spisni, G. L. Rossi, and H. Rüterjans. 2002. Structure and backbone dynamics of apo- and holo-cellular retinol-binding protein in solution. *J. Biol. Chem.* **277:** 21983–21997.
26. Mittag, T., L. Franzoni, D. Cavazzini, G. L. Rossi, and U. L. Günther. 2005. Novel insights into the mechanism of retinol binding by cellular retinol-binding protein. *In* Structure, Dynamics and Function of Biological Macromolecules and Assemblies, NATO Science Series: Life and Behavioural Sciences. J. D. Puglisi, editor. IOS Press, Amsterdam, The Netherlands. 109–122.
27. Mittag, T., L. Franzoni, D. Cavazzini, B. Schaffhausen, G. L. Rossi, and U. L. Günther. 2006. Retinol modulates site-specific mobility of apo-cellular retinol-binding protein to promote ligand binding. *J. Am. Chem. Soc.* **128:** 9844–9848.
28. Lu, J., C-L. Lin, C. Tang, J. W. Ponder, J. L. F. Kao, D. P. Cistola, and E. Li. 1999. The structure and dynamics of rat apo-cellular retinol-binding protein II in solution: comparison with the X-ray structure. *J. Mol. Biol.* **286:** 1179–1195.
29. Winter, N. S., J. M. Bratt, and L. J. Banaszak. 1993. Crystal structures of holo and apo-cellular retinol-binding protein II. *J. Mol. Biol.* **230:** 1247–1259.
30. Lu, J., C-L. Lin, C. Tang, J. W. Ponder, J. L. F. Kao, D. P. Cistola, and E. Li. 2000. Binding of retinol induces changes in rat cellular retinol-binding protein II conformation and backbone dynamics. *J. Mol. Biol.* **300:** 619–632.
31. Levin, M. S., E. Li, and J. I. Gordon. 1990. Structure-function analyses of mammalian cellular retinol-binding proteins by expression in *Escherichia coli*. *Methods Enzymol.* **189:** 506–520.
32. Malpeli, G., C. Folli, D. Cavazzini, G. Sartori, and R. Berni. 1998. Purification and fluorescent titration of cellular retinol-binding protein. *Methods Mol. Biol.* **89:** 111–122.
33. Li, E., B. Locke, N. C. Yang, D. E. Ong, and J. I. Gordon. 1987. Characterization of rat cellular retinol-binding protein II expressed in *Escherichia coli*. *J. Biol. Chem.* **262:** 13773–13779.
34. Elviri, L., I. Zagnoni, M. Careri, D. Cavazzini, and G. L. Rossi. 2001. Non-covalent binding of endogenous ligands to recombinant cellular retinol-binding proteins studied by mass spectrometric techniques. *Rapid Commun. Mass Spectrom.* **15:** 2186–2192.
35. Wishart, D. S., C. G. Bigam, J. Yao, F. Abildgaard, H. J. Dyson, E. Oldfield, J. L. Markley, and B. D. Sykes. 1995. ^{1}H, ^{13}C and ^{15}N chemical shift referencing in biomolecular NMR. *J. Biomol. NMR.* **6:** 135–140.
36. Lücke, C., F. Zhang, H. Rüterjans, J. A. Hamilton, and J. C. Sacchettini. 1996. Flexibility is a likely determinant of binding specificity in the case of ileal lipid binding protein. *Structure.* **4:** 785–800.
37. Wüthrich, K. (1986) NMR of amino acid residues and mononucleotides. *In* NMR of Proteins and Nucleic Acids. John Wiley and Sons, New York. 13–25.
38. Wishart, D. S., B. D. Sykes, and F. M. Richards. 1992. The chemical shift index: a fast and simple method for the assignment of protein secondary structure through NMR spectroscopy. *Biochemistry.* **31:** 1647–1651.
39. Careri, M., L. Elviri, A. Mangia, I. Zagnoni, F. Torta, D. Cavazzini, and G. L. Rossi. 2006. Mass spectrometry techniques for detection of ligand-dependent changes in the conformational flexibility of cellular retinol-binding protein type I localized by hydrogen/deuterium exchange. *Rapid Commun. Mass Spectrom.* **20:** 1973–1980.
40. Careri, M., L. Elviri, I. Zagnoni, D. Cavazzini, and G. L. Rossi. 2003. Acid-induced denaturation of cellular retinol-binding proteins types I and II studied by electrospray mass spectrometry. *Rapid Commun. Mass Spectrom.* **17:** 2773–2780.

41. Tarter, M., S. Capaldi, M. E. Carrizo, E. Ambrosi, M. Perduca, and H. L. Monaco. 2008. Crystal structure of human cellular retinol binding protein II to 1.2 Å resolution. *Proteins.* **70:** 1626–1630.
42. Likić, V. A., N. Juranić, S. Macura, and F. G. Prendergast. 2000. A "structural" water molecule in the family of fatty acid binding proteins. *Protein Sci.* **9:** 497–504.
43. Pal, D., and P. Chakrabarti. 2001. Non-hydrogen bond interactions involving the methionine sulfur atom. *J. Biomol. Struct. Dyn.* **19:** 115–128.
44. Lipscomb, L. A., N. C. Gassner, S. D. Snow, A. M. Eldridge, W. A. Baase, D. L. Drew, and B. W. Matthews. 1998. Context-dependent protein stabilization by methionine-to-leucine substitution shown in T4 lysozyme. *Protein Sci.* **7:** 765–773.
45. Lu, J., D. P. Cistola, and E. Li. 2003. Two homologous rat cellular retinol-binding proteins differ in local conformational flexibility. *J. Mol. Biol.* **330:** 799–812.
46. Herr, F. M., E. Li, R. B. Weinberg, V. R. Cook, and J. Storch. 1999. Differential mechanisms of retinoid transfer from cellular retinol binding proteins types I and II to phospholipid membranes. *J. Biol. Chem.* **274:** 9556–9563.
47. Wootan, M. G., and J. Storch. 1994. Regulation of fluorescent fatty acid transfer from adipocyte and heart fatty acid binding proteins by acceptor membrane lipid composition and structure. *J. Biol. Chem.* **269:** 10517–10523.
48. Hsu, K-T., and J. Storch. 1996. Fatty acid transfer from liver and intestinal fatty acid-binding proteins to membranes occurs by different mechanisms. *J. Biol. Chem.* **271:** 13317–13323.
49. Thumser, A. E. A., J. Tsai, and J. Storch. 2001. Collision-mediated transfer of long-chain fatty acids by neural tissue fatty acid-binding proteins (FABP): studies with fluorescent analogs. *J. Mol. Neurosci.* **16:** 143–150.
50. Thumser, A. E. A., and J. Storch. 2000. Liver and intestinal fatty acid-binding proteins obtain fatty acids from phospholipid membranes by different mechanisms. *J. Lipid Res.* **41:** 647–656.
51. Rademacher, M., A. W. Zimmerman, H. Rüterjans, J. H. Veerkamp, and C. Lücke. 2002. Solution structure of fatty acid-binding protein from human brain. *Mol. Cell. Biochem.* **239:** 61–68.
52. Muga, A., D. P. Cistola, and H. H. Mantsch. 1993. A comparative study of the conformational properties of *Escherichia coli*-derived rat intestinal and liver fatty acid binding proteins. *Biochim. Biophys. Acta.* **1162:** 291–296.
53. Lücke, C., D. Lassen, H-J. Kreienkamp, F. Spener, and H. Rüterjans. 1992. Sequence-specific ^{1}H-NMR assignment and determination of the secondary structure of bovine heart fatty-acid-binding protein. *Eur. J. Biochem.* **210:** 901–910.
54. Wishart, D. S., B. D. Sykes, and F. M. Richards. 1991. Relationship between nuclear magnetic resonance chemical shift and protein secondary structure. *J. Mol. Biol.* **222:** 311–333.